MZ-35, a new layered pentasil borosilicate synthesized in the presence of large alkali cations

MZ-35, a new layered pentasil borosilicate synthesized in the presence of large alkali cations

Rossella Arletti[a], Enrico Mugnaioli[b], Ute Kolb[b,c], Francesco Di Renzo[d,*]

[a]Department of Earth Science, University of Turin, Via Valperga Caluso 25, 10125 Torino, Italy

[b]Institute of Physical Chemistry, Johannes Gutenberg University Mainz, Welderweg 11, 55099 Mainz, Germany

[c]Institute of Applied Geosciences, Darmstadt University of Technology, Schnittspahnstrasse 9, 64287 Darmstadt, Germnay

[d]Institut Charles Gerhardt Montpellier, UMR 5253 CNRS-UM2-ENSCM-UM1, 8 Rue Ecole Normale, 34296 Montpellier, France

*Corresponding author. Tel.: +33 607508148.

E-mail address: direnzo@enscm.fr (F. Di Renzo).

Abstract

A new layered borosilicate has been synthesized in the presence of cesium and sodium cations and its structure has been solved by a combination of automated diffraction tomography (ADT) and X-ray powder diffraction (XRPD). MZ-35 has a composition $NaCs_2[BSi_7O_{16}(OH)_2]$ 6 H_2O and features space group P-4m2. The unusually small unit cell (a 7.3081 Å, c 10.7520 Å) is shared by two random-stacked configurations of the structure: a network of connected pentasil units related to the layer of RUB-18 and a

bidimensional checkerboard of intersecting ladders of 4-membered rings. The two configurations are related by the simple face-sharing inversion of a hydroxyl-bearing tetrahedron.

Keywords

Automated electron diffraction tomography; Rietveld structure refinement; layered borosilicate; 4-MR ladders; face-sharing terahedra

1. Introduction

Layered sodium silicates and crystalline silicic acids are a class of minerals which includes several members whose structure has not yet been solved [1]. The interest of these materials as barrier phases in composite materials for adsorption processes and fire retardants and as precursor of intercalation compounds [2] has motivated the development of procedures for the synthesis of analogs of natural-occurring minerals or for the production of new synthetic phases. The research on the subject has taken a faster pace after the discovery of bidimensional precursors in the synthesis of several specific zeolites [3-6]. Beyond their interest in the orientation of the structure of tridimensional zeolites [7, 8], these layered silicates have proven to be a useful source of porous catalytic materials after treatments of delamination [9, 10] or pillaring [11].
The formation of these synthetic phases requires the presence of specific organic templates. In the case of the synthesis of tridimensional silicates, large alkali cations have been shown to be able to replace some organic cations [12]. From this point of view, the formation of RUB-18, a representative layered silicate [13, 14], is somehow puzzling. Some published recipes of RUB-18 require the presence of sodium, cesium

and organic cations in the synthesis medium [15]. However, sodium is the only cation incorporated in the phase formed [16]. Such a selectivity of incorporation brought us to investigate in which synthesis conditions a large alkali cation like cesium could play a structure-directing role in the formation of layered silicates.

2. Experimental

2.1. Synthesis procedure

The reagents used in the syntheses were NaOH from Prolabo, pentahydrate tetramethylammonium (TMA) hydroxide from Fluka, cesium hydroxide 50 % solution and borax $Na_2B_4O_7 \cdot 10\ H_2O$ from Aldrich, precipitated silica 175MP from Rhône-Poulenc and Ludox HS-40 from DuPont. MZ-35 was obtained by a synthesis system of composition 0.359 Na_2O / 0.093 Cs_2O / 0.002 Al_2O_3 / 0.116 B_2O_3 / 1 SiO_2 / 16 H_2O. Borax and silica 175MP were stirred overnight in the soda solution. After addition of the cesium hydroxide solution the synthesis batch was sealed in a stainless steel vessel and heated at 115 °C for 6 days. The solid phase was separated by cycles of centrifugation and washing.

2.2. Composition analyses

Electron microprobe analysis was carried out using an ARLSEMQ instrument in wavelength dispersive mode, operating at 15 kV and with a beam current of 20 nA and diameter of 30 μm;counting times of 5, 10, and 5 s. on high background, peak, and low background, respectively were used. A pellet of 10 mg of powdered MZ-35 sample was prepared by applying a pressure of 10 tons mï 2. Data acquisition and processing were

performed using the PROBE program [17]. Water content was determined by thermogravimetric analysis on a 10 mg sample in a Netzsch TG209C thermal balance operating at 5 K/min up to 900°C in air flow.

2.3. Transmision Electron Microscopy (TEM) and Automated Diffraction Tomography (ADT) analysis

For TEM and Automated Diffraction Tomography (ADT) analysis the sample was dispersed in ethanol using an ultrasonic bath and sprayed on carbon-coated copper grids. The measurements were carried out with a FEI TECNAI F30 S-TWIN transmission electron microscope working at 300 kV using a FISCHIONE tomography holder. TEM images and nano electron diffraction patterns were acquired with a CCD camera (14-bit GATAN 794MSC). Scanning transmission electron microscopy (STEM) images were acquired by a FISCHIONE high angular annular dark field (HAADF) detector. Elemental analysis was done by energy disperse X-ray (EDX) spectroscopy and quantified within Emispec ESVision software.

Three dimensional electron diffraction acquisition and analysis were performed using the recently developed ADT method [18]. Acquisition was performed by the semi-automatic procedure described in ref. [19]. The ADT experimental parameters are provided in Table 1. Within this procedure, the crystal is tilted in steps of 1° and nano electron diffraction patterns are collected sequentially. Therefore the patterns cover the whole possible tilt range of the microscope goniometer and the crystal doesn't need to be oriented along low-index crystallographic directions. A condenser aperture (C2) of 10 mm and high spot size were used in order to produce a semi-parallel beam of 50 nm in diameter and reduce the electron dose rate on the sample. Crystal position is tracked

in STEM mode. In order to improve reflection intensity integration, ADT was coupled with precession of the electron beam (precession electron diffraction, PED) [20], performed using a NanoMEGAS DigiStar unit. The precession angle was kept at 1.2°. ADT data were processed using ADT3D software package coupled with self-developed Matlab scripts [21, 22]. Starting from a stack of not-oriented diffraction patterns it is possible to reconstruct the three dimensional diffraction volume, display it by a 3D rendering and calculate the unit cell vectors (cell parameters and orientation matrix). It is finally possible to index and integrate the reflection intensities and compile them into an *hkl* file. E.s.d was assumed equal to ãI. These intensities were used for finding the *ab-initio* structural model by direct methods implemented in the software SIR2008 [23]. Intensities were assumed proportional to F_{hkl}^2 neglecting residual dynamical effects.

2.4. X-ray powder Diffraction

The XRPD experiment was performed at the SNBL1 (BM01a) beamline at ESRF, in the Debyeï Scherrer geometry. The sample was placed in a 0.3 mm quartz capillary mounted on a goniometric spinning head and the diffraction pattern was collected in 180 seconds on a MAR350 detector (pixel dimensions 150μm) with a fixed wavelength of 0.70 Å and a sample-detector distance of 221mm. One-dimensional diffraction patterns were obtained by integrating the two dimensional images with the program FIT2D [24]. Rietveld profile fitting was performed using the GSAS package [25] with the EXPGUI interface [26].

Starting coordinates for the refinement were taken from TEM structural solution (see below). The background curve was fitted by a Chebyshev polynomial with 20 coefficients. The pseudo-Voigt profile function proposed by Thomson et al. was applied

[27], and the peak intensity cut-off was set to 0.1% of the peak maximum. The following strategy was used for structural refinements: (i) the scale factor, the zero-shift, and the unit cell parameters were allowed to vary for all refinement cycles (from the correlation matrix we can rule out the presence of significant correlation effects among zero-shift scale factor and the structural parameters); (ii) after the initial refinement cycles, the refined structural parameters for each data histogram were: fractional coordinates for all atoms (soft restraints were applied to the Tï O distances [Siï O = 1.60(2)ï 1.63(2)] and the weight was gradually decreased after the initial stages of refinement, down to a final weight of 10), occupancy factors for extra-framework sites and thermal isotropic displacement factors for all atoms (the isotropic displacement parameters were constrained with the same value for all tetrahedral cations, a second value for all framework O atoms, a third value for the OH groups of the framework);(iii) occupancy factors and isotropic thermal displacement factors for extra-framework sites were varied in alternate cycles. The details of the structural refinement are given in Table 2.

2.5. Nuclear magnetic resonance

29Si MAS NMR spectra were recorded on an ASX 400 Bruker spectrometer using 9.4T field, p/6 4ls pulses with 60 s repeating time, 6 kHz spinning.

3. Results

The chemical analysis of MZ-35 by EMPA (average of 15 point analyses) indicated a mass composition Na_2O 2.92%, Cs_2O 28.46% , Al_2O_3 1.61%, B_2O_3 4.03%, SiO_2 52.35%.

The thermal gravimetry pattern of the sample (Figure 1) presented a sharp loss of mass with a maximum around 150 °C followed by a slower loss of mass. Final mass is reached at about 450 °C with a total weight loss of 13.3 %.

The initial mass loss can be attributed to the loss of water molecules and the phenomenon at higher temperature to the condensation of hydroxils. Under this assumption, the combination of elemental analysis and thermal gravimetry data indicates, for a cell of eight tetrahedra (see further), a composition $Na_{0.78}\ Cs_{1.72}\ B_{0.91}\ Si_{6.86}\ Al_{0.24}\ O_{14.20}\ (OH)_{4.95} \cdot 4.72\ H_2O$.

MZ-35 consists of flat square platelets (Figure 2, Fugure 3a) up to 10 µm wide and less than 100 nm thick. As shown in Figure 2, the platelets are often stacked around a screw dislocation.

An isolated platelet, shown by preliminary diffraction probing to be a single crystal, was used for ADT data acquisition (Figure 3b). After the 3D diffraction volume reconstruction, ADT3D automatic routines allowed to determine a metrically tetragonal cell with direction 00*1* orthogonal to the platelet main facet, and *h*00 and 0*k*0 directions parallel to the platelet rims (Figure 3). A strong diffuse scattering is present along c*. Using this cell, a set of 2146 reflections were indexed and integrated with the procedure reported in ref. [22]. Due to the preferential orientation of the platelet, 00*l* reflections and nearby crystallographic directions could not be sampled as falling into the missing cone of the microscope goniometer.

On the basis of the intensities of the strongest reflections, the tetragonal Laue class P4/m was determined. No extinctions were detected in the available 3D diffraction reconstruction, but it was not possible to exclude extinctions along 00*l*. Different attempt of *ab-initio* structure solution was performed by SIR2008 [23] with space

groups belonging to extinction symbols (P ï ï ï) and ($P4_2$ï ï), tuning the cell content and the resolution limit of the diffraction information. Two comparable solutions were obtained for space group P-4 and for the related centrosymmetric P-4m2, while for the other attempted space groups no solution was achieved. P-4m2 was assumed as the correct geometry and the coordinated of the so-obtained ab-initio model were used as starting model for the XRPD refinement (Figure 4).

The borosilicate framework of MZ-35, reported in Figure 5, corresponds to a layered structure with interrupted framework. The statistic breaking of some oxygen bonds allows two possible configurations of the layers, each present in 50% of the cases. The two configurations are hereby called "1" and "bis". The atomic positions and the occupancy factors are reported in Table 3. Relevant framework distances and bond angles are reported in Table 4.

The first configuration (ñ1ò in Figure 5a) is characterized by the presence of pentasil units and is topologically equivalent to the structure of RUB-18. The basic unit is a cage of eight [TO_4] tetrahedral forming four fused five-membered rings [5^4] (Figure 6). The cage is connected to each of four neighbouring cages on the *ab* plane by two T-O-T bridges. These bridges connect the T2 atoms of four pentasil cages forming 4-membered rings (4mR) on the *ab* plane. The remaining four T1 atoms carry an hydroxyl group (OH) protruding in the interplanar space. Charge compensation is insured by the deprotonation of half hydroxyl groups, not observable in the diffraction experiment..

The second configuration (ñbisò in Figure 5b) is metrically equivalent to the pentasil configuration, but it is characterized by the breaking of the T1-O3-T1 bridges of the pentasil units. The T1 tetrahedra rotate to the T1bis position and are bonded via $O3_{bis}$ oxygen bridges to the T1bis tetrahedra originated from the opening of the neighbouring

pentasil unit. The newly formed T1bis-O3bis-T1bis bridges and the pre-existing T2-O1-T2 bridges form a bidimensional checkerboard of intersecting dreier double chains of 4 membered rings running along *a* and *b* directions.

The layers of both configurations are stacked along the *c* direction. The strong diffuse scattering along c* observed in the ADT reconstruction suggests a disordered distribution of the layers along the c axis. On the contrary, the absence of disorder along a* and b* indicate that multiple configurations inside a single layer are rare occurrences. No defined preferred distribution of B, Al and Si in the tetrahedra is observed, albeit a slightly short average T-O distance in $T1_{bis}$ tetrahedra could suggest a slight preferential occupancy of B for this site.

The charge-compensating cations Na and Cs lye in two different sites in the interlayer (Figure 7). Na is at the intersection among the mirror planes and -4 axis, (a = 0, *b* = 0, c = 0) below the 4mR formed by T2 and O1 atoms. It coordinates six H_2O molecules, four X1 (lying on the same plane at *c* = 0, with a Na-O distance 2.69 Å) and two X2 (lying at the intersection between the mirror planes perpendicular to *a* and *b*, with a Na-O distance 2.28 Å), forming a coordination octahedron. The nearly regular octahedra are linked via H-bridges to the silanol group of two adjacent silicate layers, with a distance of 2.67 Å in the configuration ñ1ò and 2.53 Å in the configuration ñbisò. Cs is located on the mirror plane perpendicular to *b* direction (*b* = 1/2) and is coordinated to two O1 framework atoms and four equivalent water molecules X1. The extraframework atoms in the interlayers space form a checkerboard in which Cs cations connect the coordination octahedral of Na. This organization of the extraframework atoms is common to both framework configurations, the pentasil configuration and the 4mR-ladder configuration.

^{29}Si MAS-NMR spectra of MZ-35 (Figure 8) present two groups of resonances centered at -98 and -106.5 ppm. The chemical shifts of these groups of bands can be interpreted by the classical correlation of Radeglia and Engelhardt between Si-O-T angle and chemical shift for tectosilicates [29]. The average T-O-T angles for the sites T1, T1bis and T2 are, respectively, 155.1, 148.3 and 145.6 degrees. A Si/B ratio 7 with a random distribution of B suggests equivalent frequencies of silica tetrahedra coordinated to Si alone and to one B, with an average decrease of the chemical shift of 2.5 ppm. In the case of the sites T1 and T1bis, corresponding to a silanol, a further decrease of 10 ppm is expected. Under these assumptions, the correlation of Radeglia and Engelhardt suggests a distribution centered around 105.9 ppm for site T2 and -99.4 ppm for the average of sites T1 and T1bis, in good agreement with the experimental shifts.

4. Discussion

The determination of the structure of MZ-35 was achieved by a combination of ADT, for determining an ab-initio model, and XRPD, for performing structure refinement. This combination was already successful for structure elucidation of complex zeolites [30], MOFs [31] and layered inorganic-organic materials [32]. As pointed out by McCusker and Baerlocher [33], electron diffraction and powder diffraction are remarkably complementary techniques and their combination is highly effective for the characterization of the strycture of nanocrystalline porous materials.

The structure of MZ-35 is strictly related to the layered silicate RUB-18, synthesised and characterized by Vortmann et al. in 1997 [16]. In fact, the layer forming the pentasil configuration of MZ-35 is topologically equivalent to the basic layer of RUB-18. The main difference between the two structures is the presence of a second different layer

configuration in MZ-35, not observed in RUB-18. This implies further differences in the sequence of layers and in the distribution of cations in the interlayers.

The nature and position of the interlayer cations fairly differs in the two layered silicates.

In RUB-18 only sodium is present as charge-compensating cations, two of them per basic pentasil unit. The cations lye in the pockets between two silicate layers and are octaedrally coordinated to the oxygen atoms of the intercalated water molecules. The NaO_6 octahedra share edges to give one-dimensional chains. MZ-35 presents two sodium and one cesium cation per basic unit, the supplementary cation providing charge-compensation for a borosilicate anion. In MZ-35, sodium octahedra ï whose vertices are occupied by 4 water molecules and 2 hydroxyls, does not share edges. Cs cations, present along with sodium in the interlayers, connect the coordination octahedra of Na. In both RUB-18 and MZ-35, the water molecules at the vertices of the octahedra are bonded to the silanols groups of the two adiacent silicate layers.

While the *a* parameters of RUB-18 and MZ-35 are very similar, the *c* parameters of the two layered silicates largely differ. In fact, while in MZ-35, along the c direction, a single unit cell includes only one tetrahedral layer, in RUB-18, due to the presence of an 4_1 screw axis, four layers, related by symmetry operations, are stacked along the c direction. As a consequence of the layer distribution and of the larger cation content, the c parameter of the unit cell of RUB-18 is more than four time longer than the c parameter of MZ-35.

The main difference between the structures of RUB-18 and MZ-35 is the presence in MZ-35 of a second configuration formed by criss-crossed 4MR-ladders. This configuration corresponds to the opening of the T1-O3-T1 bond of the pentasil unit and

the formation of an alternative bond between T1 tetrahedra of opposite basic units. In the case of a reconstructive transformation, this represents a face-sharing-tetrahedra process [34]. Indeed, the tetrahedra T1 and T1bis of the two configurations share the plane through three vertices and only differ by their orientation by respect to this mirror plane: towards the pentasil unit for the configuration "1" and towards the opposite unit for the configuration "bis". The opening of the pentasil unit allows a significant relaxation of the lattice. The Si1-O2-Si2 angles of the internal bonds of the pentasil units in the configuration "1" of MZ.35 are strained to 159° (as is the case for the corresponding bonds in RUB-18), while the Si1bis-O2-Si2 bonds of the ladder-chain configuration "bis" are relaxed to 148°.

Couples of configurations characterized by face-sharing tetrahedra are not uncommon in layered silicates. A typical example are the staggered or eclipsed orientations across the twin layers of, respectively, latiumite and tuscanite, two anion-bearing layered aluminosilicates [35].

The presence of a large alkali cation seems to be critical for the formation of the MZ-35. The synthesis is indeed highly selective for the incorporation of cesium, as the molar ratio Cs/Na 2 of MZ-35 is much higher than the Cs/Na ratio 0.25 of the synthesis batch. Large alkali cations are very effective templates for the formation of borosilicate structures [12] through a local stabilisation of trigonal boron in the synthesis system. As shown in the case of the formation of borosilicates in the presence of tetraalkylammonium cations [36], trigonal boron in alkaline solution is liable to nucleophilic attack by silicate anions, the first step for the formation of networks of $[BO_4]$ and $[SiO_4]$ tetrahedra. It can also be observed that the synthesis batch which leads

to the formation of the layered MZ-35 structure is significantly more alkaline than the syntheses batches of cesium-templated boron-bearing tectosilicates [12].

5. Conclusions

The present interest on the potential of layered silicates as precursors of catalytic materials is at the basis of the research for the synthesis of new structures with diverse topology and composition. The formation of MZ-35 is an example of the extension to layered structures of the use of large alkali cations as templates of borosilicate structures, a possible alternative to the use of organic templates already demonstrated in the case of tectosilicates.

The combination of electron diffraction and powder diffraction is extremely effective for the study of crystal structures. In the case of layered silicates with very small crystal size in a given direction or with intrinsic disorder, only such a powerful tool allows to solve new structures. In the case of MZ-35, the resolution of the structure was made especially difficult by the presence of randomly-stacked layers with two different configurations in crystals whose thickness corresponds to less than one hundred unit cells.

When the structure of MZ-35 is considered in the context of other structures of zeolite-related materials, the presence of two configurations sharing the same unit cell is an example of the easy conversion of silicate structures by face-sharing inversion of tetrahedra. Such a mechanism, well known in the modification of some zeolite structures by thermal treatment or compression, is less frequently observed in the synthesis of silicate materials and it is probaly favoured by the larger freedom of

rotation of tetrahedra in hydroxyl-bearing layered materials, when compared with the higher stability of the network of tectosilicates.

6. Acknowledgments

ADT experiments were supported by Stiftung Rheinland Pfalz für Innovation. The authors are grateful to Marie-France Driole for experimental support and Roger Dutartre for the scanning electron microscopy.

References

[1] W. Schwieger, G. Lagaly, in: S.M. Auerbach, K.A. Carrado, P.K. Dutta (Eds.), Handbook of layered materials, Marcel Dekker, New York 2004, pp. 521-618.

[2] G. Lagaly. Adv. Colloid Interface Sci. 11 (1979) 105-148.

[3] R. Millini, G. Perego, W.O. Parker, Jr., G. Bellussi, L. Carluccio, Microporous Materials 4 (1995) 221-230.

[4] L. Schreyeck, P. Caullet, J.C. Mougenel, J.L. Guth, B. Marler. Microporous Materials 6 (1996) 259-271.

[5] S. Zanardi, A. Alberti, G. Cruciani, A. Corma, V. Fornes, M. Brunelli, Angew. Chem. Int. Ed. 43 (2004) 4933-4935.

[6] M. Choi, K. Na, J. Kim, Y. Sakamoto, O. Terasaki, R. Ryoo, Nature 461 (2009) 246ï 250.

[7] W.J. Roth, J. Cejka, Catal. Science Technol. 1 (2011) 43-53.

[8] W.J. Roth, P. Nachtigall, R.E. Morris, P.S. Wheatley, V.R. Seymour, S.E. Ashbrook, P. Chlubna, L. Grajciar, M. Polozij, A. Zukal, O. Shvets, J. Cejka, Nature Chem. 5 (2013) 628-633.

[9] A. Corma, V., Fornes, S.B. Pergher, Th.L.M. Maesen, J.G. Buglass, Nature 396 (1998) 353-356.

[10] A. Corma, V. Fornes, J. Martēnez-Triguero, S. B. Pergher, J. Catal. 186 (1999) 57ï 63.

[11] W.B. Fan, P. Wu, S. Namba, T.Tatsumi, Angew. Chemie Int. Ed. 43 (2004) 236-240.

[12] F. Di Renzo, M. Derewinski, G. Chiari, J. Plévert, M.F. Driole, F. Fajula, P. Schulz, Microporous Materials 6 (1996) 151-157.

[13] H. Gies, B. Marler, S. Vortmann, U. Oberhagemann, P. Bayat, K. Krink, J. Rius, I. Wolf, C. Fyfe, Microp. Mesop. Mater. 21 (1998) 183-197.

[14] T. Ikeda, Y. Oumi, K. Honda, T. Sano, K. Momma, F. Izumi, Inorg. Chem. 50 (2011) 2294-2301.

[15] U. Müller, H. Gies, S. Siegmann, S. Vortmann, DE 19543848 A1 (1997).

[16] S. Vortmann, J. Rius, S. Siegmann, H. Gies, J. Phys. Chem. B 101 (1997) 1292-1297.

[17] J.J. Donovan, M.L. Rivers, in: J.R. Michael, P. Ingram (Eds.), Microbeam analysis, San Francisco Press, san Francisco 1990, pp. 66ï 68.

[18] U. Kolb, E. Mugnaioli, T.E. Gorelik, Cryst. Res. Technol. 46 (2011) 542-554.

[19] U. Kolb, T. Gorelik, C. Kübel, M.T. Otten, D. Hubert, Ultramicroscopy 107 (2007) 507-513.

[20] R. Vincent, P.A. Midgley, Ultramicroscopy 53 (1994) 271-282.

[21] U. Kolb, T. Gorelik, M.T. Otten, Ultramicroscopy 108 (2008) 763-772.

[22] E. Mugnaioli, T. Gorelik, U. Kolb, Ultramicroscopy 109 (2009) 758-765.

[23] M.C. Burla, R. Caliandro, M. Camalli, B. Carrozzini, G.L. Cascarano, L. De Caro, C. Giacovazzo, G. Polidori, D. Siliqi, R. Spagna, J. Appl. Crystallogr. 40, (2007) 609-613.

[24] A.P. Hammersley, S.O. Svensson, M. Hanfland, A.N. Fitch, D. Häusermann, High Pressure Res. 14 (1996) 235-248.

[25] A.C. Larson, R.B. Von Dreele, GSAS-General Structure Analysis System. Report LAUR 86-748, Los Alamos National Laboratory, Los Alamos 1996.

[26] B.H. Toby, J. Appl. Crystallogr. 34 (2001) 210-213.

[27] P. Thomson, D.E. Cox, J.B. Hastings, J. Appl. Crystallogr. 20 (1987) 79-83.

[28] E.F. Pettersen, T. D. Goddard, C. C. Huang, G. S. Couch, D. M. Greenblatt, E. C. Meng, T. E. Ferrin, J. Comput. Chem. 25 (2004) 1605-1612.

[29] R. Radeglia, G. Engelhardt, Chem. Phys. Lett. 114 (1985) 28-30.

[30] J. Jiang J., J.L. Jorda, J. Yu, L.A. Baumes, E. Mugnaioli, M.J. Diaz-Cabanas, U. Kolb, A. Corma, Science 333 (2011) 1131-1134.

[31] M. Feyand, E. Mugnaioli, F. Vermoortele, B. Bueken, J.M. Dieterich, T. Reimer, U. Kolb, D. de Vos, N. Stock, Angew. Chem. Int. Ed. 124 (2012) 10519-10522.

[32] G. Bellussi, E. Montanari, E. Di Paola, R. Millini, A. Carati, C. Rizzo, W.O.J. Parker, M. Gemmi, E. Mugnaioli, U. Kolb, S. Zanardi, Angew. Chem. Int. Ed. 51 (2012) 666-669.

[33] L.B. McCusker, Ch. Baerlocher, Z. Kristallogr. 228 (2013) 1-10.

[34] A. Alberti, A. Martucci, Microp. Mesop. Mater. 141 (2011) 192-198.

[35] M. Mellini, S. Merlino, G. Rossi. Am. Miner. 62 (1977) 1114-1120.

[36] R. de Ruiter, J.C. Jansen, H. van Bekkum, Zeolites 12 (1992) 56-62.

Table 1. ADT experimental parameters.

Tilt range	-60° / +55°
Total sample reflections	882
Symmetrical independent reflections	121
Maximum resolution	1.1 Å
Independent reflection coverage	84%
R_{sym}	23.7%
Overall U	0.096 $Å^2$
Residual R(F) (by SIR2008)	21.4%

Table 2**:** X-Ray powder diffraction refinement parameters.

Space Group	P-4m2
Cell Parameters	a=7.3081(5) c=10.7520(9)
Composition	$NaCs_2[BSi_7O_{14}(OH)_4]$ 6 H_2O
Rwp	0.02
Rp	0.02
R/F2**	0.03
N° Variables	53
N° Observations	1185

Table 3**:** Refined atomic positions, occupancy factors and displacement parameters ($Å^2$) of MZ-35

	x/a	**y/b**	**z/c**	**Occupancy**	**Uiso**
T1	0.285(1)	0.50	-0.287(1)	0.519(8)	0.033(2)
T1bis	0.50	0.213(1)	0.302(1)	0.496(7)	0.033(2)
T2	0.2072(6)	0.7928(6)	0.50	1.00	0.033(2)
O1	0.00	0.759(1)	0.453(1)	1.00	0.055(3)
O2	-0.325(1)	0.751(1)	0.3804(7)	1.00	0.055(3)
O3	-0.50	0.50	0.242(3)	0.519(8)	0.055(3)
O3bis	0.00	0.50	0.742(3)	0.496(7)	0.055(3)
OH	0.50	0.158(2)	0.172(2)	0.519(8)	0.020(7)
OHbis	0.50	0.310(3)	0.170(2)	0.496(7)	0.020(7)
Cs	0.00	0.50	0.2054(2)	0.989(3)	0.060(1)
Na	0.00	1.0	0.00	0.99(2)	0.106(9)
X1	0.260(2)	0.260(2)	0.00	1.1(1)	0.039(4)
X2	0.00	0.00	0.212(2)	1.2(1)	0.069(8)

Table 4**:** Ti O framework distances (Å), O-T-O bond angles and cations coordination of MZ-35

		Distance
T1	**O2**	1.64(1)
	O2	1.64(1)
	O3	1.64(4)
	OH	1.56(2)
T2	**O1**	1.615(5)
	O1	1.615(5)
	O2	1.580(0)
	O2	1.580(0)
T1bis	**O2**	1.554(8)
	O2	1.554(8)
	O3bis	1.62(1)
	OHbis	1.60(2)

Cs	**O1**	3.269(2)
	X1 [x4]	3.400(1)
Na	**X1 [x4]**	2.69(2)
	X2 [x2]	2.28(2)

Angle	
O2-T1-O2	102.0(10)
O2-T1-O3	104.9(10)
O2-T1-OH	113.1(7)
O2-T1-O3	109.4(10)
O2-T1-OH	113.1(7)
O3-T1-OH	109.6(17)

O2-T1bis-O2	110.4(9)
O2-T1bis-O3bis	108.8(7)
O2-T1bis-OHbis	114.1(6)
O2-T1bis-O3bis	108.8(7)
O2-T1bis-OHbis	114.1(6)
O3bis-T1bis-OHbis	99.9(16)

O1-T2-O1	112.5(10)
O1-T2-O2	110.7(5)
O1-T2-O2	103.2(5)
O1-T2-O2	103.2(5)
O1-T2-O2	110.7(5)
O2-T2-O2	116.7(9)

Figure captions

Figure 1. TG (thick line) and DTG (thin line) curves of MZ-35.

Figure 2. Scanning electron micrograph of MZ-35.

Figure 3. (a) Dark-field STEM image of typical MZ-35 platelets. (b) STEM image of the platelet used for the best ADT acquisition. (c) 3D diffraction reconstruction by ADT data viewed along c*. Main crystallographic directions are parallel with main crystal rims. (d) 3D diffraction reconstruction viewed along b*, showing diffuse scattering along c*. Reciprocal space visualization are made by UCSF-Chimera [28].

Fig. 4. X-ray powder diffraction refinement of MZ-35.

Fig. 5. Projection of configuration 1 (a) and configuration ñbisò (b) of MZ-35 structure along [100] and [001].

Fig. 6. Basic unit of the configuration 1 of MZ-35.

Fig.7**.** Projection of the MZ-35 structure along the [100] direction. Extraframework positions: cesium: dark blue; sodium: red; water X1: light blue; water X2: grey.

Figure 8. ^{29}Si MAS-NMR spectra of MZ-35.

Figure 1

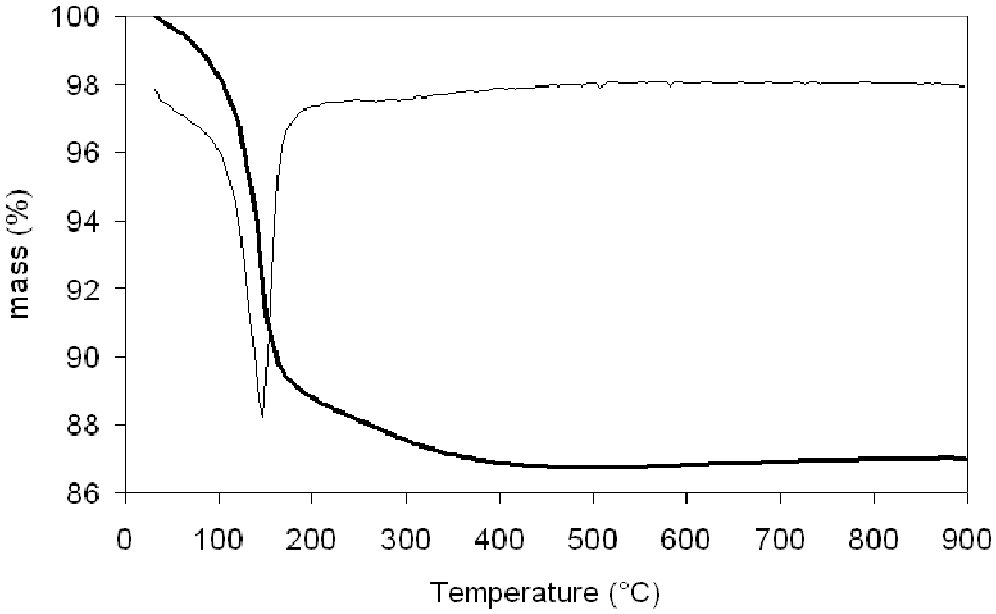

Figure 2.

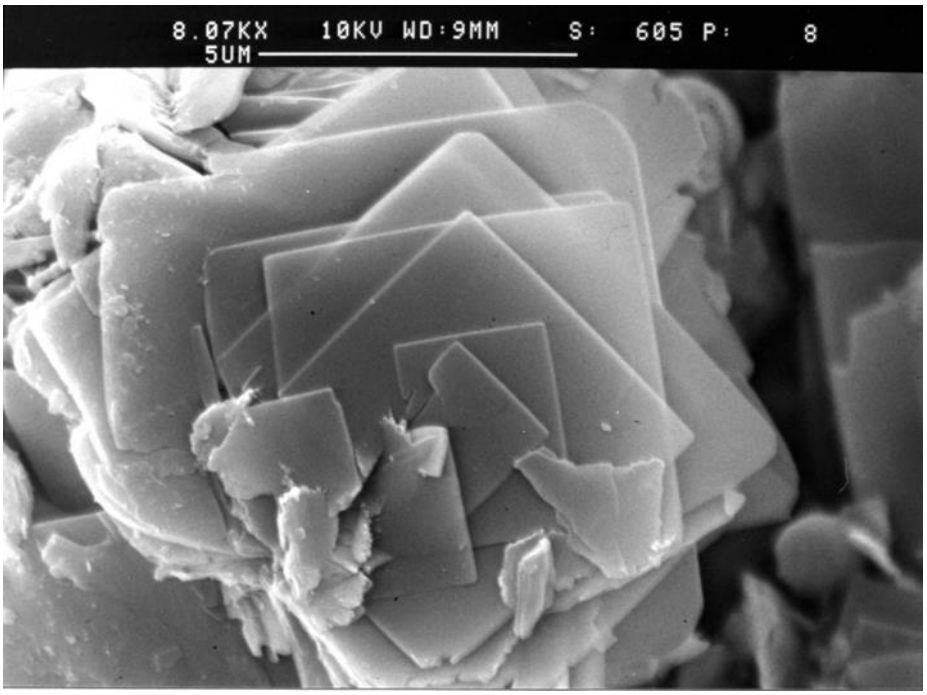

Figure 3

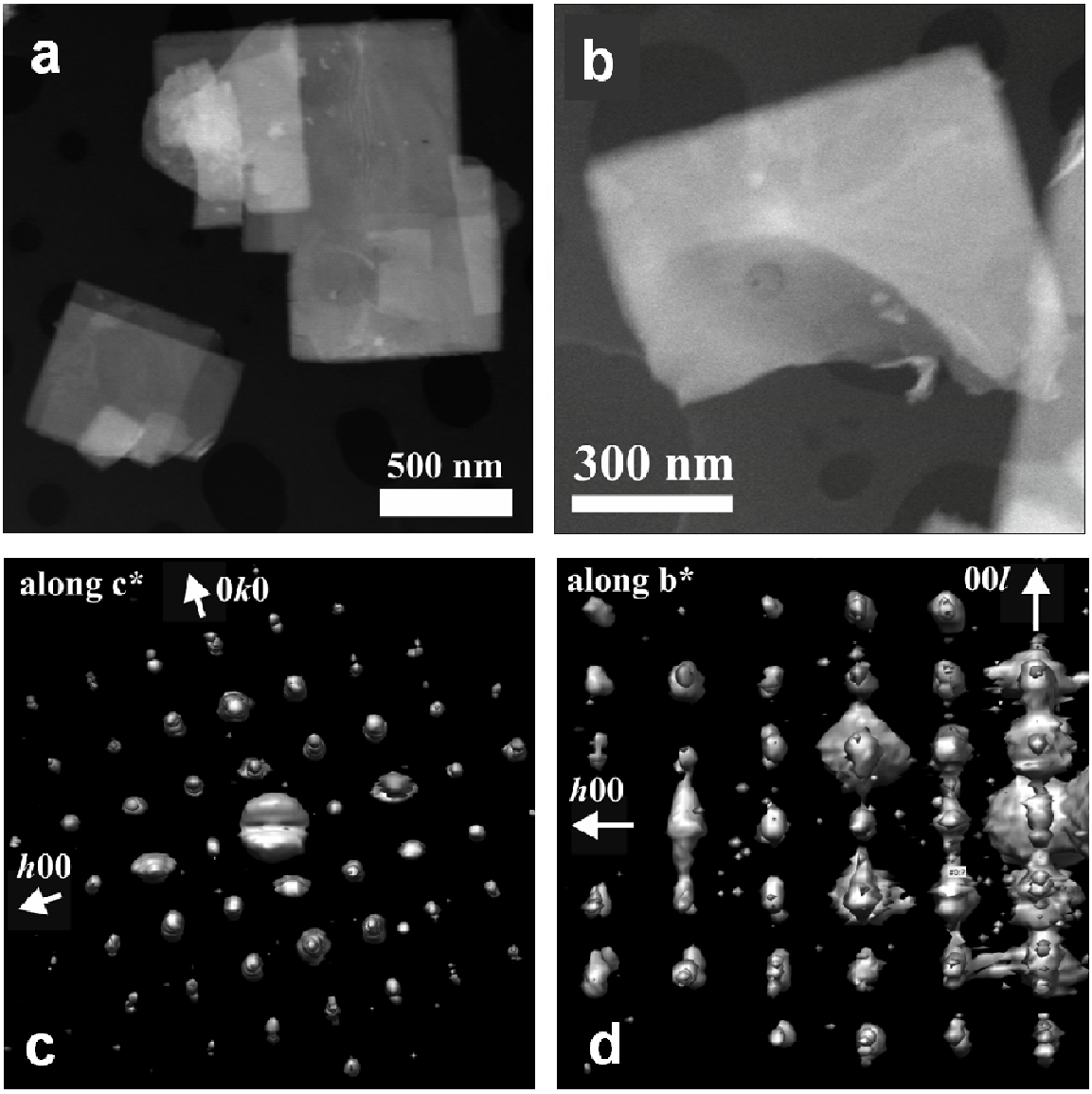

Figure 4

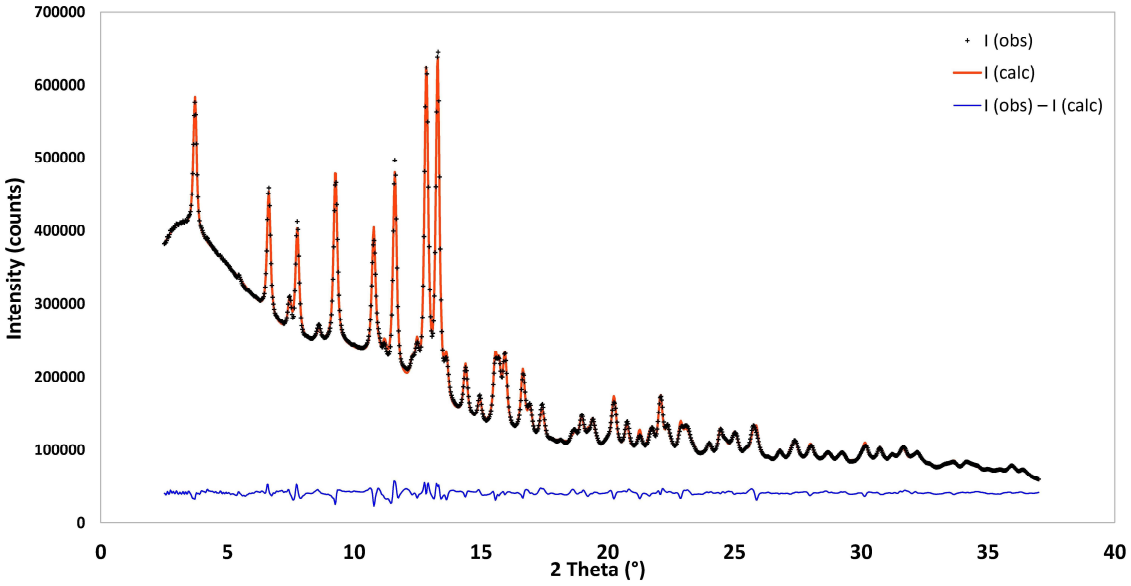
I (obs)
I (calc)
I (obs) – I (calc)
Intensity (counts)
700000
600000
500000
400000
300000
200000
100000
0
0
5
10
15
20
25
30
35
40
2 Theta (°)

Figure 5

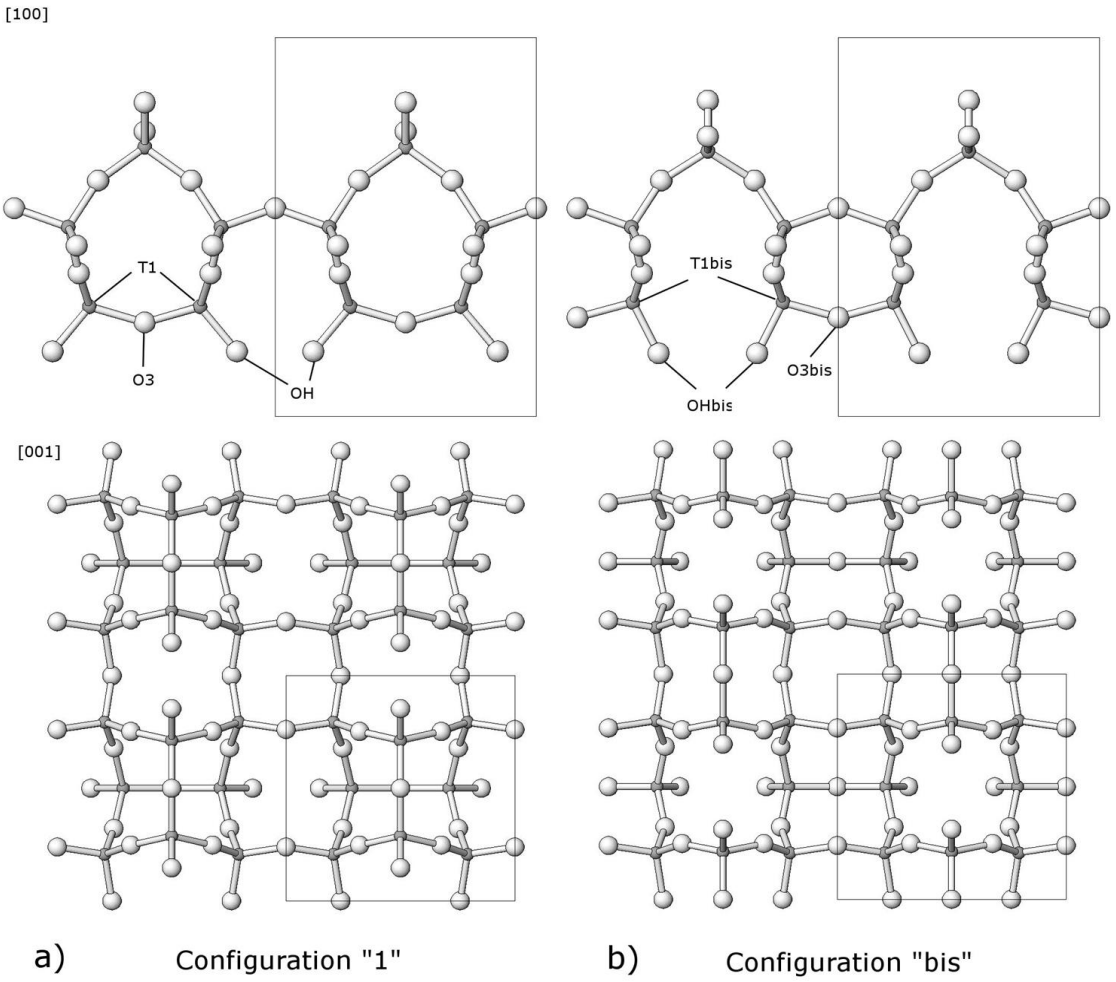

Figure 6

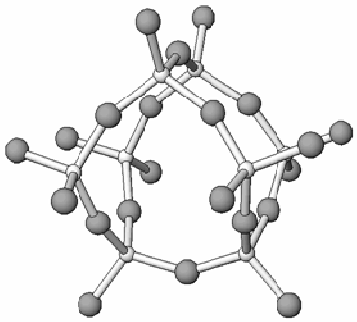

Figure 7

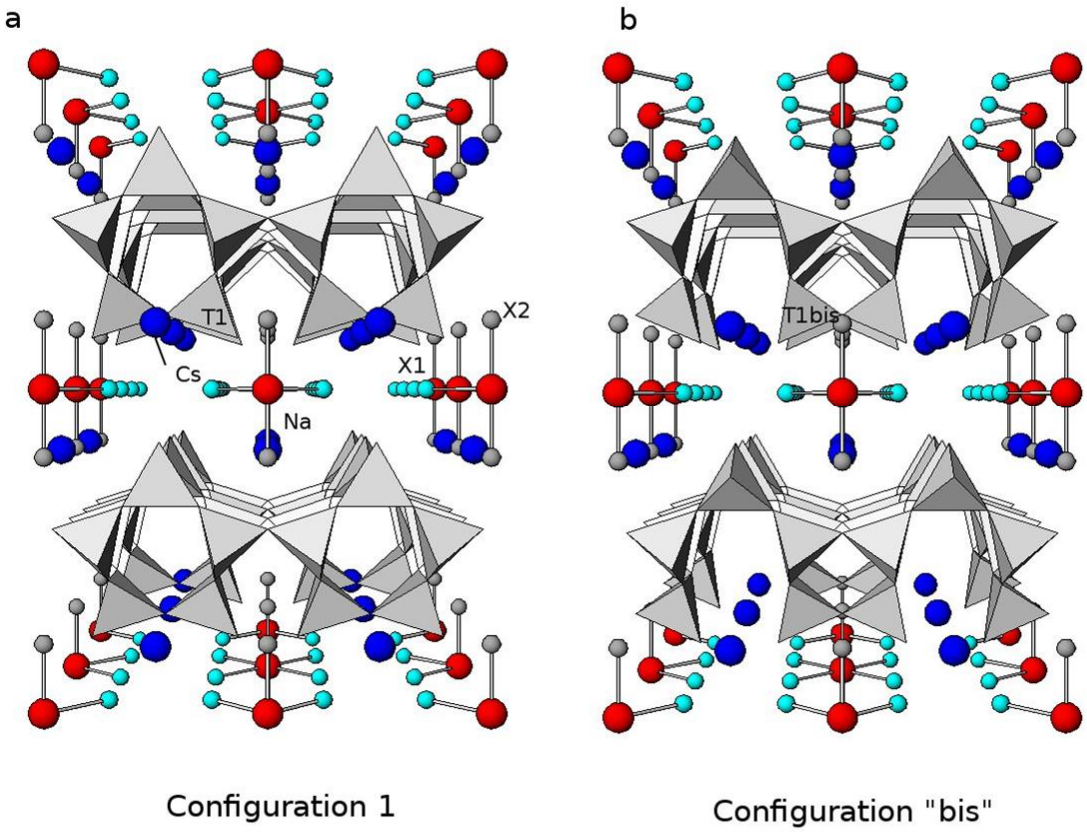

Figure 8